Investigation of polarization-independent wide-angle metamaterial inspired ISM-band absorber

Kanwar Preet Kaur* & Trushit Upadhyaya

Department of Electronics and Communication Engineering, Chandubhai S Patel Institute of Technology,
Charotar University of Science and Technology, Changa, Anand 388 421, India

In this paper, the polarization independent wide angle ISM-band metamaterial absorber structure has been investigated for various geometrical parameters along with the practical demonstration. The presented structure has been numerically simulated using full wave electromagnetic simulator exhibiting absorption peak of 99.42% at 2.48 GHz. The effects of variations in geometrical parameters have been manifested by designing and experimentally verifying two absorber structures with modified parameters, yielding near unity single absorption of 99.89% at 2.4 GHz while dual absorption of 97.2% and 98.1% at 1.76 GHz and 2.48 GHz, respectively. The unit cell of proposed absorber structure comprises of a closed ring resonators engraves on a grounded FR4 dielectric substrate. The simplicity of design imparts effortless fabrication and design symmetry provides polarization insensitivity. Additionally, it has been observed that the proposed structure could achieve high absorption of 90% up to 45° of incident transverse electric wave and up to 60° of transverse magnetic wave attains high absorption of 99%. The optimized absorber structures have been practically demonstrated using waveguide measurement technique and the outcomes are in good agreement with the numerically simulated results.

Keywords: Metamaterials, Metamaterial absorber, Ring resonators, Polarization

1 Introduction

Perfect metamaterial absorbers have gained significant interest among researchers from past few years due to attractive metamaterial properties such as negative permeability, negative permittivity, simultaneously negative permeability and permittivity, negative refractive index, to name a few, which are difficult to attain by naturally existing materials[1-4]. A phenomenal involvement in the metamaterial-based research has been evolved after Shelby *et al.*[5] in 2001 experimentally demonstrated existence of negative refractive index in the metamaterial. Some of the potential applications of metamaterials includes super lens[6], electromagnetic cloaking[7,8], antennas[9-12] and filters[13-15]. Electromagnetic metamaterials are generally artificial composite materials whose properties are altered by changing geometrical parameters of sub-wavelength unit cell. The sub-wavelength unit cells constituted by metamaterial[16] have dimensions typically lesser than $\lambda/4$, where λ is the operating wavelength and are considered to have periodic nature. The first metamaterial absorber was proposed by Landy[17] in 2008 having maximum absorbance of 96% (simulated) and 88% (experimental) at 11.5 GHz. This structure consists of several sub-wavelength unit cells with each unit cell consisting of electric ring resonator (ERR), dielectric substrate, and metal cut wires. The magnetic and electric response thereby the effective permeability (μ_{eff}) and effective permittivity (ε_{eff}) of the absorber structure are changed by engineering the geometries of the structure. Subsequently, many metamaterial based absorber designs have been proposed, among which includes compact, ultra-thin[18-20], multiband[21-24], wideband and wide angle[25,26], bandwidth enhanced[27-29] and polarization-insensitivity[30-32].

In this article finite element method (FEM) based full wave high frequency structure simulator (HFSS) software is used to obtain the effective parameter values. The absorption efficiency of the proposed absorber structure is obtained as 99.42% at 2.48 GHz. It is shown numerically as well as experimentally that the same structure could be designed for 2.4 GHz with absorption of 99.89% by merely changing the geometrical parameters of the original structure. It is demonstrated numerically and practically that by increasing the number of concentric ring the number

*Corresponding author (E-mail: kanwarpreet27@gmail.com)

of absorption band increases on optimization of the unit cell. Thus, a dual-band absorber is designed to exhibit absorption efficiency of 97.2% and 98.1% at 1.86 GHz and 2.48 GHz, respectively. Also, effects of variation in geometrical parameters on absorption response are studied. Furthermore, numerical computations are performed to justify the polarization insensitivity of the suggested structure. The absorption response for various incidence angles is inspected for justification of wide angle absorption. The absorption mechanism is analyzed by studying equivalent circuit model, surface current density and electric field distributions. The proposed absorber is designed for ISM band applications with selection of annular shape for the unit cell design as its n-fold symmetry significantly aids in polarization insensitivity and imparts ease in fabrication. The main aim of the proposed article is to design and analyze all the aspects of the metamaterial-based absorber to maximally utilize the ambient ISM-band RF energy. This is done by building energy harvester and the efficiency of any energy harvester rests on its ability to absorb energy. Energy harvester with unity absorber is going to transfer maximum power to a load ensuring dissipation of the total power across the load whereby it is collected for further applications.

2 Absorption Mechanism

According to the effective medium theory, absorption mechanisms of metamaterial absorbers (MMA) relies on the independent control of complex effective medium parameters: electric permittivity ($\varepsilon(\omega)$) and magnetic permeability ($\mu(\omega)$) of the homogeneous absorber structure to create the perfect absorption[33]. The prime characteristic of any electromagnetic absorber is its absorption efficiency because the amount of energy available being absorbed is often small[34] and is defined by the equation:

$$A(\omega) = 1 - R(\omega) - T(\omega) \qquad ...(1)$$

where $A(\omega)$ is absorbance $R(\omega) = |S_{11}(\omega)|^2$ is the reflectance, and $T(\omega) = |S_{21}(\omega)|^2$ is the transmittance which are dispersive in nature. To optimize the design of the absorber structure it is necessary to maximize the absorption coefficient by minimizing $R(\omega)$ and $T(\omega)$. To obtain a absorber with 100% absorption efficiency, a perfect MMA, both $T(\omega)$ and $R(\omega)$ should be reduced to zero. In practice, it is quite difficult to reduce both $T(\omega)$ and $R(\omega)$ to zero.

However, absorber structure with a perfect electric conductor (PEC) having skin depth much lesser than its thickness brings $T(\omega)$ nearly to zero. Whereas, $R(\omega)$ is brought roughly to zero by matching impedance of the structure to the surrounding space. The real and imaginary parts of $\varepsilon(\omega)$ and $\mu(\omega)$ are varied independently such that $\varepsilon(\omega) \approx \mu(\omega)$. At this moment impedance of the structure becomes equal to the free space impedance at desired range of frequencies[18]. Aforementioned parameters are derived from the transmission coefficients and reflection coefficients[35] as follows:

$$z(\omega) = \sqrt{\frac{(1 + S_{11}(\omega))^2 - S_{21}^2(\omega)}{(1 - S_{11}(\omega))^2 - S_{21}^2(\omega)}} \qquad ...(2)$$

and

$$n(\omega) = \frac{1}{kd} \cos^{-1}\left[\frac{1}{2S_{21}}(1 - S_{11}^2(\omega) + S_{21}^2(\omega))\right] \qquad ...(3)$$

where, kd is known as path length and is defined as $2\pi d/\lambda$ with d representing the thickness of a single sub-wavelength unit cell of the absorber structure. $n(\omega)$ and $z(\omega)$ are related to $\varepsilon(\omega)$ and $\mu(\omega)$ by the following relations

$$\varepsilon(\omega) = \frac{n(\omega)}{z(\omega)} \quad and \quad \mu(\omega) = n(\omega)z(\omega) \qquad ...(4)$$

The reflection coefficients or return loss $S_{11}(\omega)$ and transmission coefficients or insertion loss $S_{21}(\omega)$ are computed with numerical simulators and later would be measured with an experimental setup.

3 Proposed Absorber Design

The geometry of the proposed MMA is shown in Fig. 1. This structure has three significant layers. Top layer of the sub-wavelength unit cell consisting of a closed ring resonator (CRR), middle layer is FR4 dielectric substrate and PEC forms the bottom layer. FR4 material is utilized, as dielectric substrate for the proposed absorber as its lossy characteristics further aids in absorption of electromagnetic waves (EM). The conductivity (σ) of copper sheet is 5.8×10^7 S/m and has thickness (t_c) of 0.035 mm. The relative permittivity (ε_r) and dielectric loss tangent ($\tan\delta$) of FR4 substrate are 4.4 and 0.02, respectively. More the thickness of substrate, higher is the absorption bandwidth, lower is the absorption efficiency (Fig. 13(a)). Hence, dielectric substrate thickness (t_s) is selected as 1.6 mm for single-band MMA while

2.4 mm for dual-band MMA. The optimized geometrical parameters of the proposed absorber unit cell are as follows: a = 27.2 mm, r = 11.5 mm, w = 1.1 mm and g = 2.1 mm. These optimized parameters make size of the proposed absorber unit cell to be less than $\lambda/4$ thereby satisfying the effective-homogeneity condition[16].

4 Numerical Computation Results

The proposed MMA structure is simulated using periodic boundary conditions for normal incident of the EM. Floquet port excitation of HFSS is utilized for applying the periodic boundary conditions. The electric field is along X-axis while magnetic field is along Y-axis with incoming EM wave in the direction normal (along Z-axis) to the surface of the MMA. Theoretically, $T(\omega)$ perfectly reduces to zero as the substrate is entirely coated with copper plate. Hence, the relation in Eq. (1) reduces to take the form as shown below:

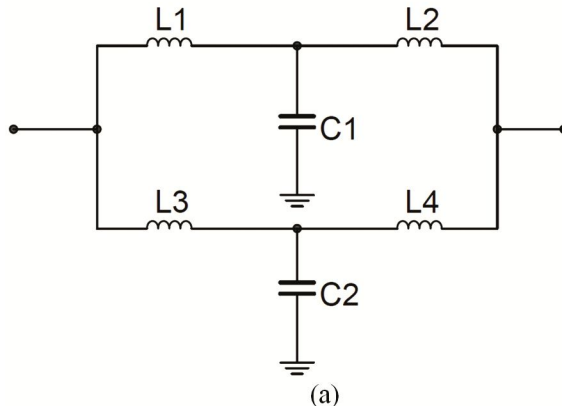$$A(\omega) = 1 - \left| S_{11}(\omega) \right|^2 = 1 - R(\omega) \qquad \ldots (5)$$
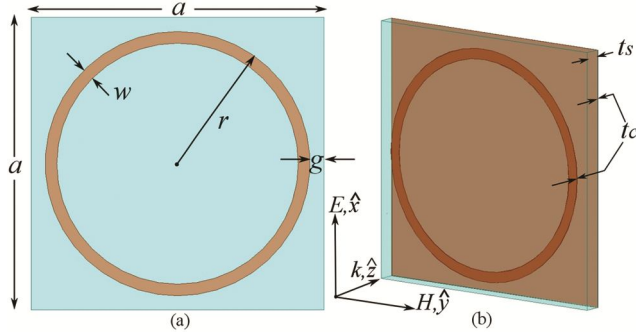
Fig. 1 – Geometries of single unit cell of the proposed 2.48 GHz MMA: (a) front view and (b) perspective view.

Thus, the only parameter to be controlled for maximum absorption is $R(\omega)$ which must be minimized. The minimization of $R(\omega)$ is done by matching impedance of the structure to the free space impedance. This results in the absorption of 99.42% with reflection coefficient of -22.36 dB at 2.48 GHz frequency as illustrated in Fig. 2. The T-network equivalent circuit for the proposed absorber 2.48 GHz MMA is presented in Fig. 3(a). The gap capacitances have been excluded from calculation as the gaps between the rings are greater than 1 mm. The values of L (L_1=L_2=L_3=L_4=L) and C (C_1=C_2=C) are obtained from literature[36] as L=43.15 nH and C=0.186 pF, respectively. By incorporating the ohmic losses the calculated reflection coefficient is in good agreement with the simulated reflection coefficient. The comparative graphs for the two reflection coefficients are shown in Fig. 3(b).

Using the retrieval algorithm[35] the retrieved effective normalized impedance [$z_{eff}(\omega)$] of the
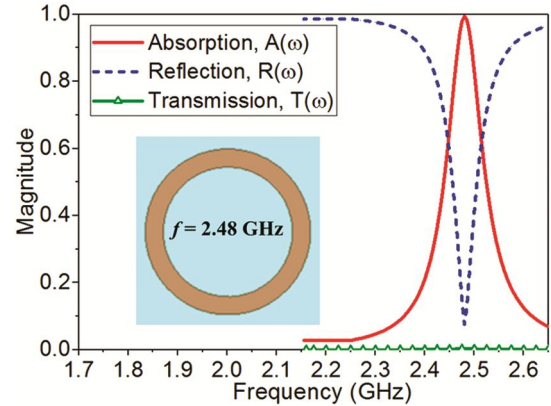

Fig. 2 – Simulated results for absorption, reflection and transmission of the proposed 2.48 GHz MMA under normal incidence.
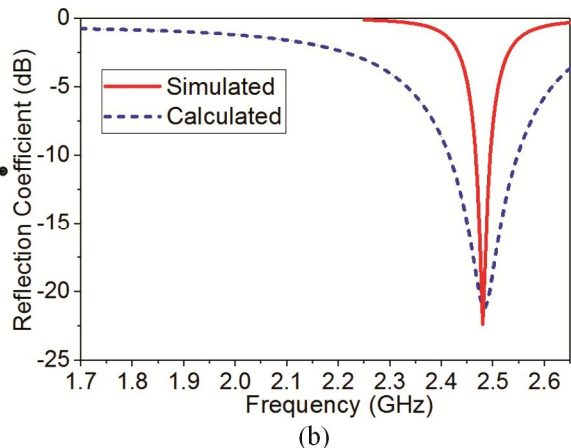

Fig. 3 – (a) T-network equivalent circuit of proposed 2.48 GHz MMA and (b) comparison between simulated and calculated reflection coefficient of the proposed 2.48 GHz MMA.

proposed MMA is presented in Fig. 4(a). It is conclude that the real part of the normalized $z_{eff}(\omega)$ is close to unity implying that the effective impedance of the proposed absorber structure nearly matches the free space impedance. Furthermore, at this frequency imaginary part of $z_{eff}(\omega)$ is near zero thereby minimizing the reflection. Under this matching condition, the imaginary component of $n(\omega)$ attains high value at the target frequency as depicted in Fig. 4(b). $Re(n_{eff})$ should be less than zero for negative index, whereas $Im(n_{eff})$ should be high for absorption[37,38]. Larger the $Im(n_{eff})$ more is the attenuation of wave inside the structure. Figure 5 shows the variation of effective permittivity and effective permeability of the proposed 2.48 GHz absorber which is retrieved from[35] with respect to frequency. It is apparent that the values of real and imaginary parts of ε_{eff} and μ_{eff} are approximately equal at the target absorption frequency of 2.48 GHz making effective impedance of the proposed absorber

structure to approximately match with the free space impedance. To achieve higher absorption rate the structure is constructed with 2×4 arrays having periodicity of a mm and substrate dimension is kept equivalent to the inner aperture dimension of the waveguide (WR-430) as illustrated in Fig. 6.

Figure 7 depicts distribution of the surface current density on top and bottom face of the proposed MMA at the absorption frequency of 2.48 GHz. It is evident that the surface current density directions on the top face of the proposed MMA are anti-parallel with that of surface current density directions on bottom face. The circulating current loops are formed due to these anti-parallel currents and are perpendicular to the incident magnetic field. The magnetic excitation thus created, influences $\mu_{eff}(\omega)$ of the proposed structure. On the other hand, $\varepsilon_{eff}(\omega)$ is controlled by inducing electric excitation through incident electric field on the top face of the structure as shown in Fig. 8. It is noted that the induced electric field is
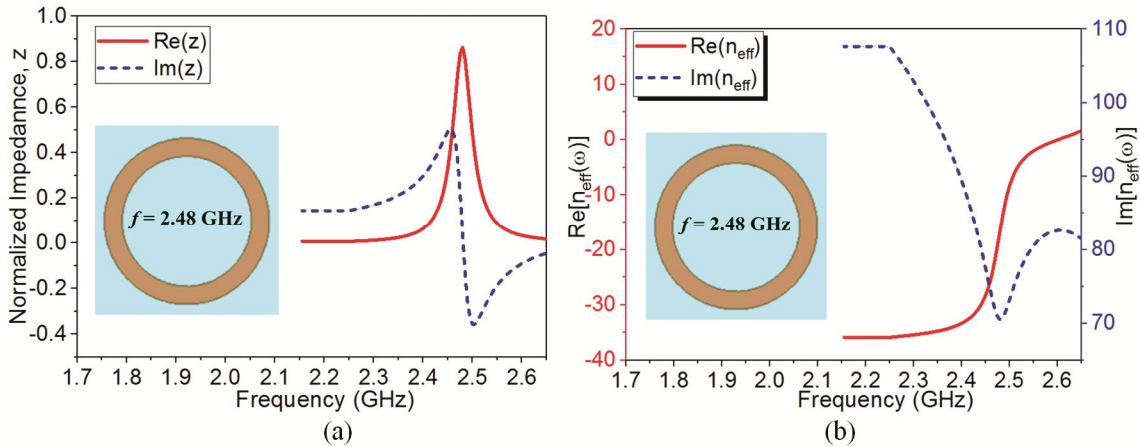

Fig. 4 – Simulated results of the proposed 2.48 GHz MMA under normal incidence for: (a) normalized impedance, z and (b) effective refractive index, n_{eff}.
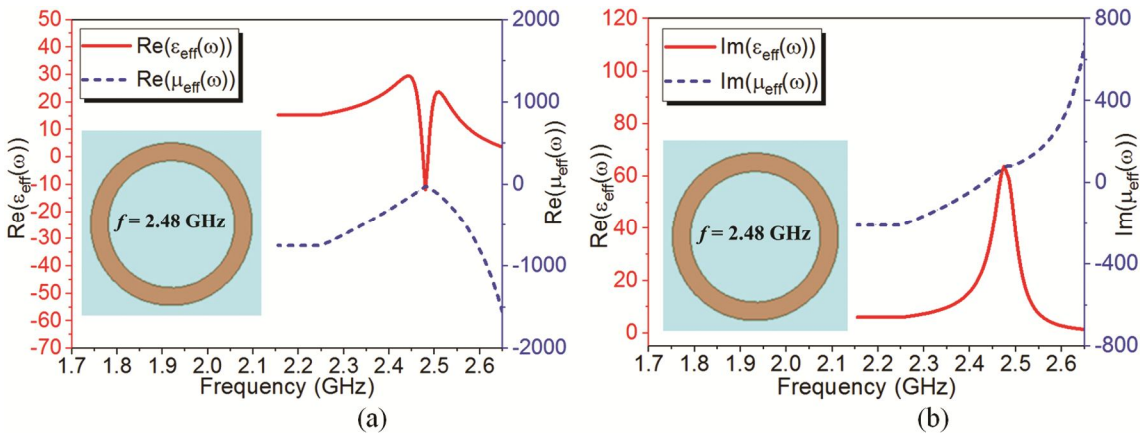

Fig. 5 – Comparison of (a) real parts of ε_{eff} and μ_{eff} and (b) imaginary parts of ε_{eff} and μ_{eff} for 2.48 GHz proposed MMA.
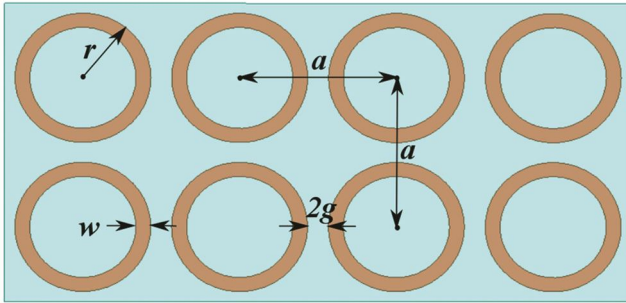
Fig. 6 – Front view geometries of array structure of the proposed 2.48 GHz MMA.

concentrated on the edges of the ring. Thus, both $\mu_{eff}(\omega)$ and $\varepsilon_{eff}(\omega)$ could be controlled simultaneously to achieve high absorption at desired frequency by altering the geometry of the unit cell.

From Fig. 9, it is observed that the absorption efficiency is above 99% at various polarization angles (ϕ) under normal incidence. The practical verification of polarization of MMA using waveguide measurement technique is done by setting different orientations of the CRR. Each rotated CRR unit cell is fabricated and tested for polarization stability[39].
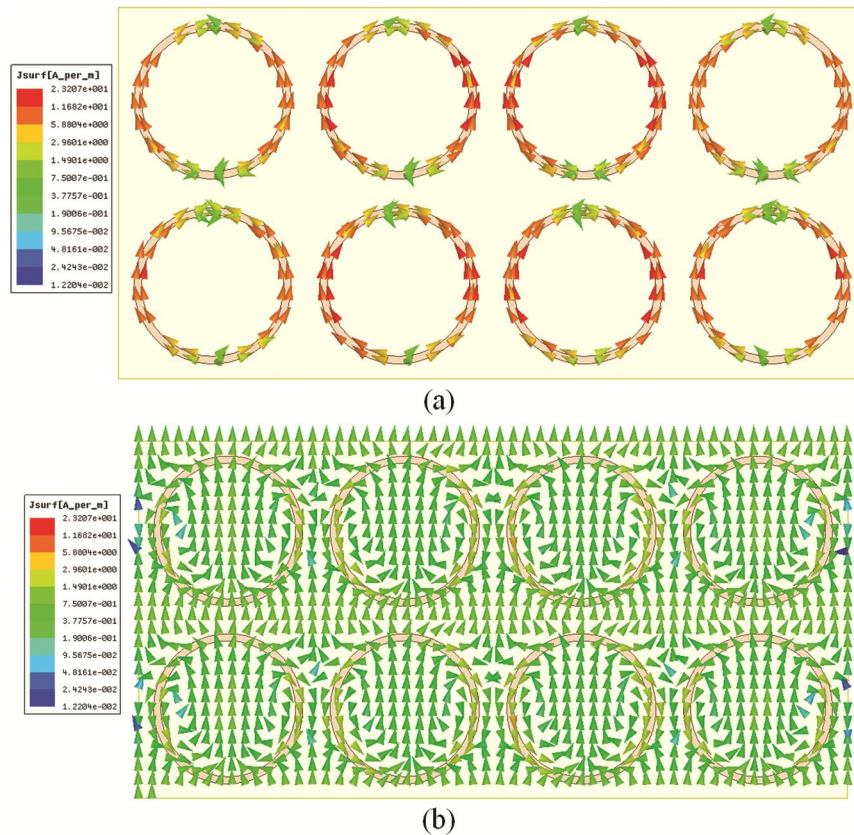

(a)

(b)

Fig. 7 – Current density distribution at 2.48 GHz: (a) top face and (b) bottom face.
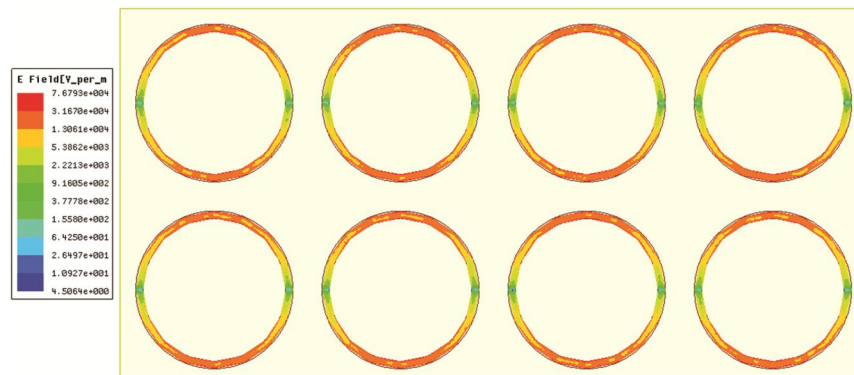

Fig. 8 – Induced electric field distributions at 2.48 GHz.

Furthermore, the effect of varying angle of oblique incidence (θ) under both transverse-electric (TE) and transverse-magnetic (TM) excitation are studied. In case of TE excitation, for fixed φ angle the direction of incident electric field is kept constant thereby varying magnetic field and wave propagation vector

by an angle θ. In contrast, for TM excitation the direction of incident magnetic field is maintained uniform while the varying other two vectors by angle θ for constant φ angle. The proposed absorber structure shows considerable simulated absorption greater than 90% for oblique incidence up to 45° for TE excitation and for TM excitation, absorption came to be about 99% up to 60° of oblique angle as illustrated in Fig. 10.
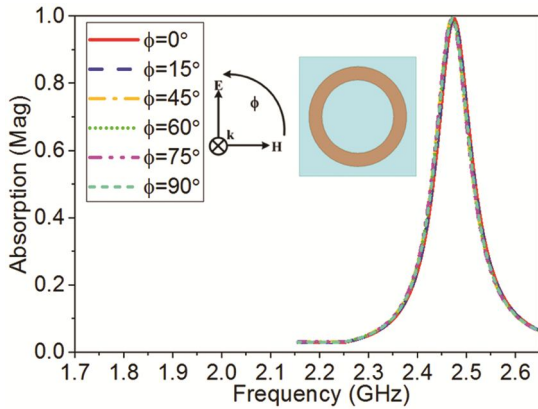
5 Parametric Variation Analysis

To further investigate the effect of geometrical parametric variations on absorption response, various parameters are changed gradually. Firstly, annular patch width (w) and gap width (g) of 2.48 GHz structure are changed gradually to observe the effect of the modifications. By observing the effect of these variations a separate MMA is designed for absorption at 2.4 GHz. The variation in w from 1.2 mm to 2 mm with steps of 0.1 mm is represented in Fig. 11(a). It is observed that as the width w is increased there are
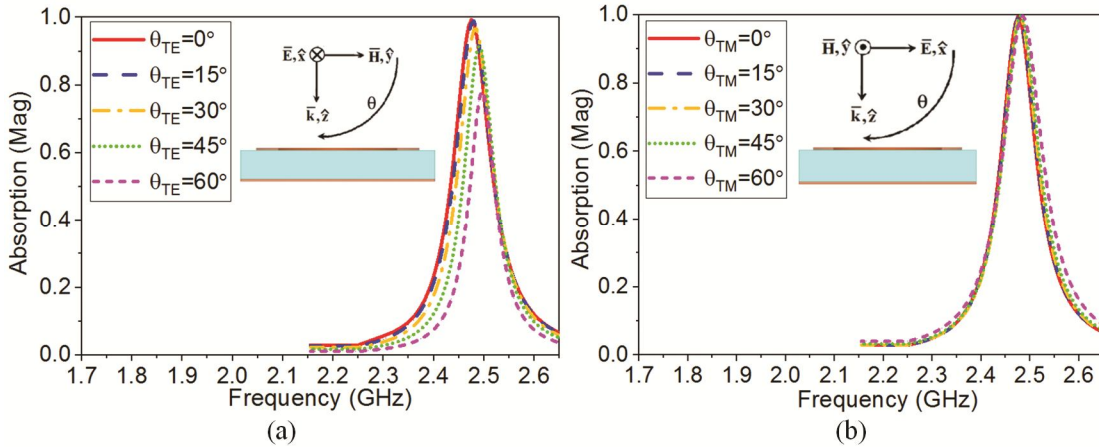

Fig. 9 – Simulated absorption response for different polarization angles under normal incidence for 2.48 GHz MMA.

(a)   (b)

Fig. 10 – Simulated absorption at 2.48 GHz with varying oblique incidence angle for: (a) TE mode and (b) TM mode.

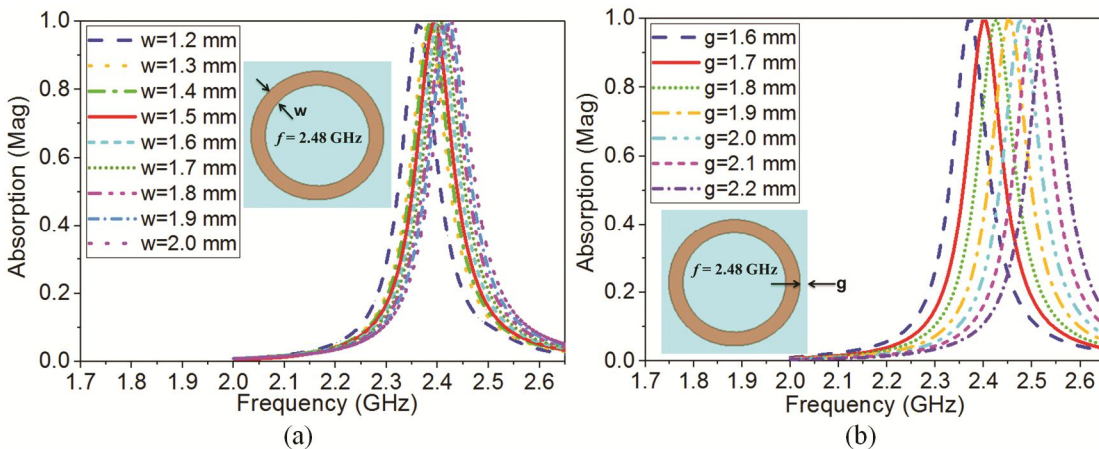(a)   (b)

Fig. 11 – Graphs depicting effect of variation of geometrical parameters in 2.48 GHz MMA (a) annular patch width (w) and (b) gap width (g).

slight shifts in the absorption frequency towards right side with consistent absorption rate of about 99%. Further, the consequence of variation in gap width g is illustrated in Fig. 11(b). It is noted as g increases from 1.6 mm to 2.2 mm with step size of 0.1 mm, frequency of each absorption response also increases progressively with near unity absorption rate. In both cases, reason behind gradual increase in absorption frequency with high absorption rate is said to be the selection of unit cell shape. Thus, by setting w and g of 2.48 GHz structure to new optimized values 99.89% of absorption takes place at 2.4 GHz with -29.71 dB of reflection coefficient. The graph for 2.4 GHz structure is depicted in Fig. 12. The values of geometrical parameters for 2.4 GHz MMA are as follows: a = 27.2 mm, r = 11.9 mm, w = 1.5 mm and g = 1.7 mm.

Figure 13(a) depicts the effect of variation in substrate height (t_s) on absorption response. It is observed that on increasing t_s the losses present in dielectric increases the imaginary part of the effective
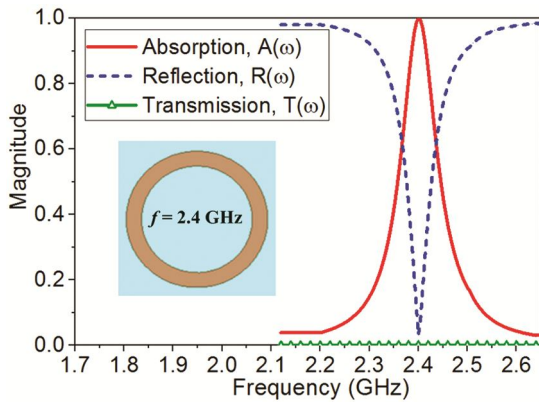
impedance thereby significantly increasing the absorption bandwidth but with reduction in absorption efficiency. However, this drawback could be eliminated by further engineering the absorber structure. Thus, it could be stated from the investigation that MMA has to be constructed on substrate with larger thickness and higher loss tangent. Finally, the effect of appending two or more concentric rings on absorption response is studied. It is noted that by increasing the number of concentric ring, the number of absorption band increases on optimization of the unit cell[24]. To justify the statement numerical computation result for two optimized concentric annular rings achieving dual-band absorption is presented in Fig. 13(b). It is observed that the absorption efficiency of 97.2% and 98.1% with reflection coefficients of -15.548 dB and -17.203 dB is obtained at 1.86 GHz and 2.48 GHz, respectively. The geometrical parameters for dual band absorber are as follows: a = 27.4 mm, R_1 = 13.5 mm, w_1 = 0.6 mm (outer annular ring), R_2 = 12.2 mm, w_2=2 mm (inner annular ring) and t_s = 2.4 mm.

For dual band absorber all the effective parameters retrieved from literature[35] is depicted in Fig. 14 and Fig. 15. It is observed that the conditions of z, n_{eff}, ε_{eff} and μ_{eff} stated for achieving high absorption in case of single band absorber (2.48 GHz) is also true for dual-band absorber. Thus, for achieving perfect absorption Re[n_{eff}] should be less than zero while Im(n_{eff}) should be positive. Additionally, Re(z_{eff})=1 and Im(z_{eff})=0; lastly, real and imaginary parts of ε should be same as real and imaginary parts of μ, respectively, for matching effective impedance for the absorber with free space impedance.

The suggested MMA is compared with the prevailing MMA designed based on ring structures at

Fig. 12 – Simulated results of the proposed 2.4 GHz MMA under normal incidence: absorption, reflection and transmission.
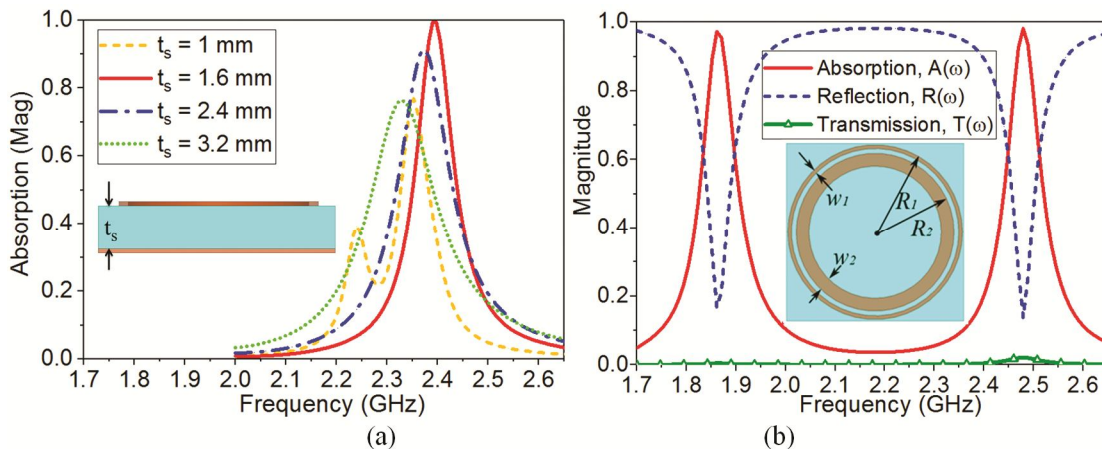

(a)

(b)

Fig. 13 – Simulated results for the geometrical parameter variations: (a) effect of variation of substrate height (t_s) and (b) dual-band MMA: absorption, reflection and transmission.

microwave frequencies in Table 1. It is concluded from Table 1 that the proposed absorber MMA has finer compactness and an extensive investigation on MMA is performed at ISM-band frequency. Thus, this article gives in-depth analysis on designing MMA with the suitable choice of unit cell design specifically based on concentric CRRs for achieving desired bandwidth, frequency, number of bands and absorption level.

6 Experimental Setup and Results

The free space measurement method[17] is the most frequently used method for experimental testing of metamaterial inspired absorber, however, the large (approximately 10λ) sample size requirement is major constrain of this method. Hence, the waveguide method[40,41] is used in presented study to test the proposed MMA as it requires a small rectangular sized sample and the testing procedure is easier to
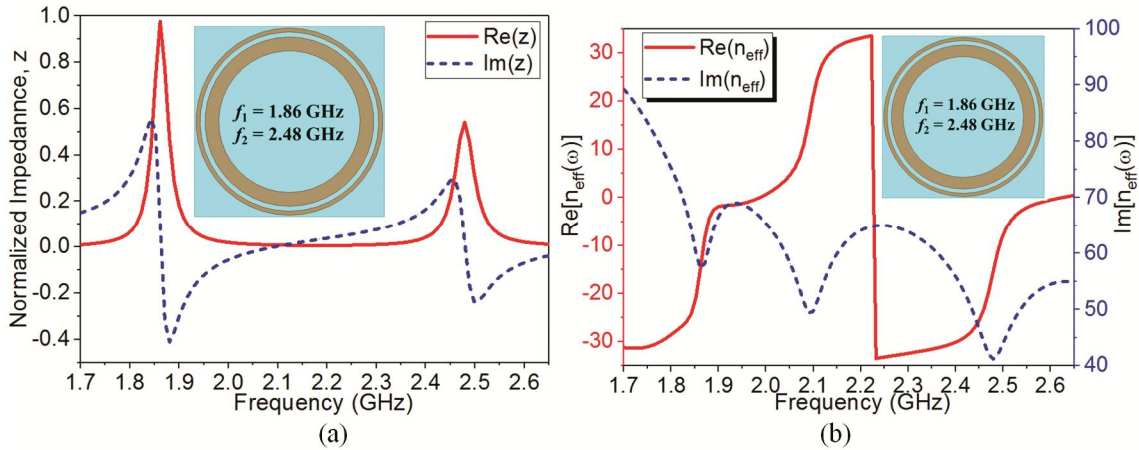

Fig. 14 – Simulated results of the proposed dual-band MMA under normal incidence: (a) normalized impedance, z and (b) effective refractive index, n_{eff}.
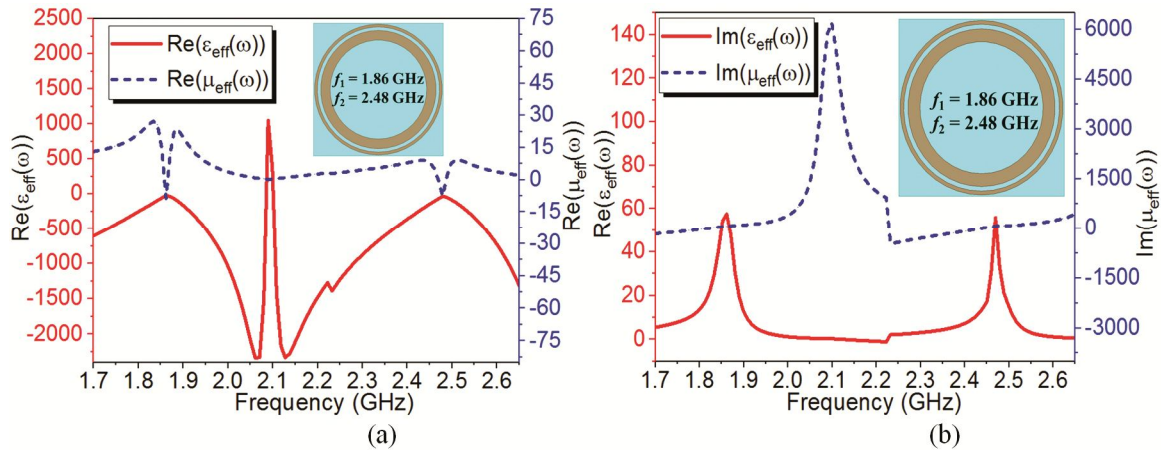

Fig. 15 – Comparison of (a) real parts of ε_{eff} and μ_{eff} and (b) imaginary parts of ε_{eff} and μ_{eff} for proposed dual-band MMA.

Table 1 – Comparison of proposed MMA with the prevailing MMA designs.

Absorber [Ref]	Unit Cell Dimensions (in mm)	Absorption Efficiency (%)	Frequency Band (GHz)	Measurement Method
[23]	20×20×0.8	98.5, 97.7, 94.8 & 96	4.34, 6.68, 8.58 & 10.64	Free-space
[24]	10×10×1	92.03, 90.46, 95.1, 91.65 & 91.1	5.28, 7.36, 9.52, 12.64 & 16.32	Free-space
[29]	6×6×1.6	95.7, 99 & 98.9	4.69, 5.19 & 7.15	
[41]	12×12×3	>90	Wideband 12.5 to 14	Waveguide
Proposed MMA	27.2×27.2×1.6 27.4×27.4×2.4	99.42 97.2 & 98.1	2.48 (Single band) 1.86 & 2.48 (Dual band)	Waveguide

carry through. Sample size is same as that of the inner aperture dimension (109.22 mm × 54.61 mm) of the waveguide. The fabricated test samples of three MMAs and complete measurement setup are depicted in Fig. 16 and Fig. 17, respectively. The practical demonstration is performed by using standard WR-430 waveguide which is connected to an Agilent N9912A vector network analyzer (VNA) via low lossy RG142 Teflon coaxial cable. The absorber sample is placed inside the waveguide and waveguide port is firmly encrusted with a metal plate to prevent any leaky wave. Thereby, the absorption efficiency is calculated by measuring $S_{11}(\omega)$ coefficient using VNA.

Figure 18(a) depicts the experimental results of reflection coefficient and absorption response for 2.48 GHz and 2.4 GHz absorber sample. The measured reflection coefficient and absorption efficiency for 2.48 GHz MMA is obtained as -22.36 dB and 99.42% at 2.454 GHz, respectively, while measured reflection coefficient of -22.51 dB and absorption of 99.44% at 2.385 GHz is obtained for 2.4 GHz MMA. The measured results of reflection coefficient and absorption response for dual band absorber sample are depicted in Fig. 18(b). The measured reflection coefficient of -17.84 dB and -17.42 dB with corresponding absorption of 98.36% and 98.49% is
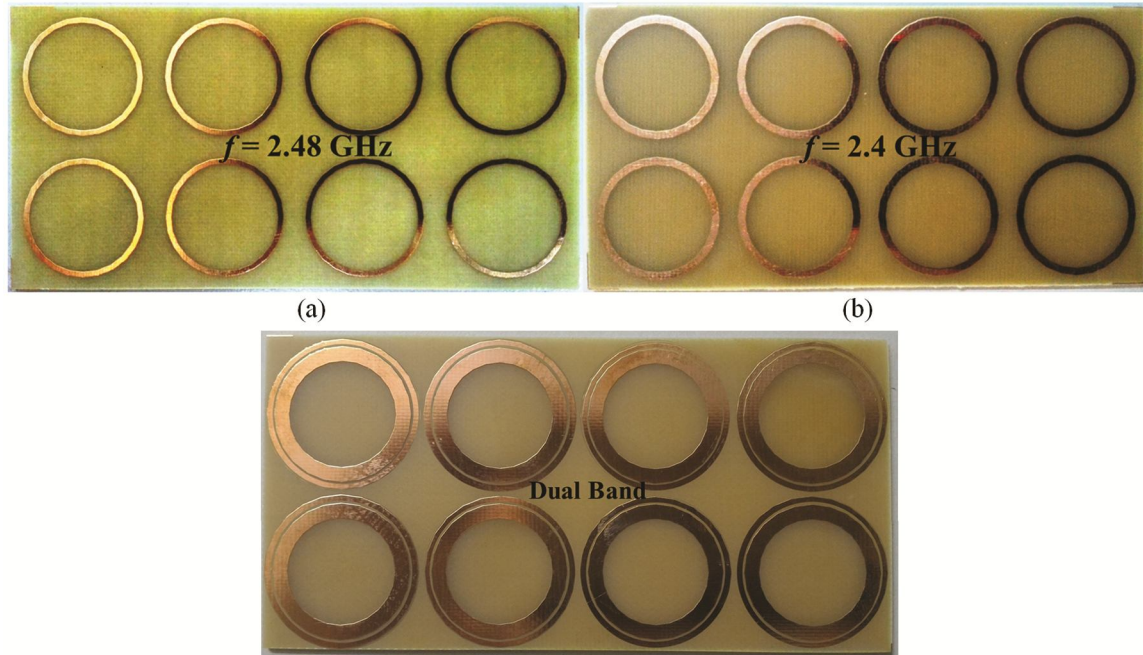

Fig. 16 – Photograph of the fabricated proposed absorber test sample: (a) 2.48 GHz MMA, (b) 2.4 GHz and (c) dual-band MMA.
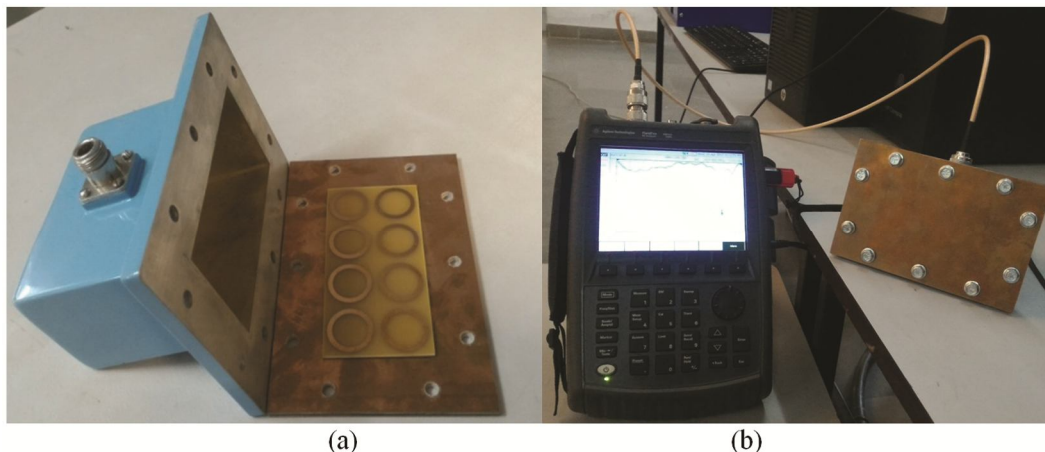

Fig. 17 – Photograph of standard waveguide and the test setup of waveguide measurement method; (a) standard waveguide with absorber sample on metal plate to firmly encrust the waveguide port and (b) complete waveguide measurement setup.
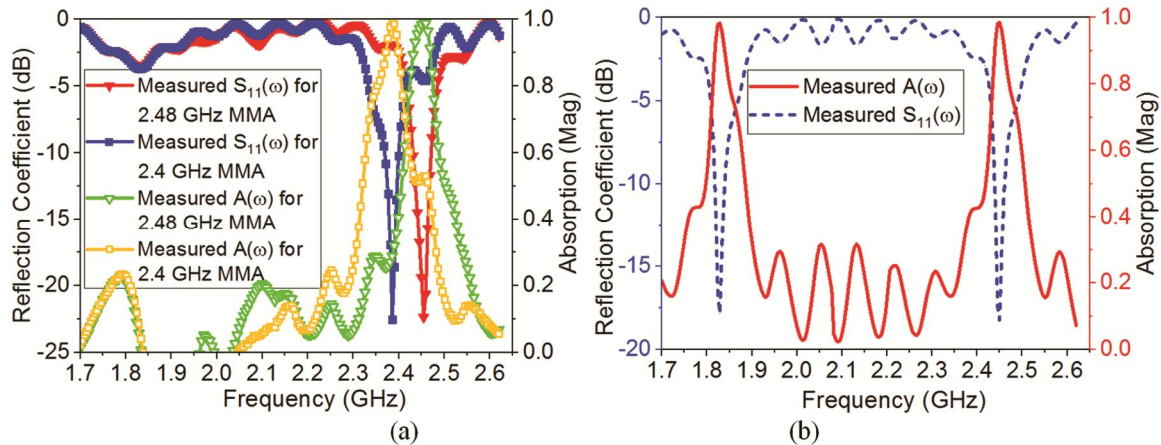
Fig. 18 – (a) Measured results for 2.48 GHz MMA and 2.4 GHz MMA and (b) measured results for dual-band absorber.

obtained for dual band MMA at 1.829 GHz and 2.449 GHz, respectively. It is noted that the experiment results are in good agreement with the simulated results. Though there are slight frequency shift of about 0.02 GHz-0.03 GHz in both of the measured reflection coefficient responses. This is due to the TE_{10} mode excitation in case of waveguide measurement[40]. This frequency shift is also aided by fabrication mismatch tolerance, cable loss and impure cost effective FR-4 substrate.

7 Conclusions

In this article, a polarization independent wide angle ISM-band metamaterial absorber has been investigated for various geometrical parameters with practical demonstrations. The presented MMA structure achieves numerical absorption of 99.42% at 2.48 GHz. By parametric analysis it is manifested that the unit cell of 2.48 GHz MMA is optimized to absorb EM signal at 2.4 GHz with 99.89% absorption efficiency by re-scaling the original structure. Also, it is shown numerically and practically that the insertion of CRR increases the absorption band proportionally. The numerically computed results and experimental outcomes of 2.48 GHz, 2.4 GHz and dual band MMA are in good agreement. The proposed 2.48 GHz structure has achieved above 99% of absorption for all polarization angles. Wide oblique incidence angle up to 45° for TE excitation with about 90% of absorption is attained and about 99% is achieved for TM excitation up to 60° of oblique angle. Moreover, in-depth numerical analysis are done to investigate the structure parameters responsible for designing MMA with the suitable choice of bandwidth, frequency, number of bands and absorption level based on concentric close ring resonator unit cell along with its equivalent circuit analysis.

References

1 Veselago V G, *Sov Phys Usp*, 10 (1968) 509.
2 Smith D R, Padilla W J, Vier D C, Nemat-Nasser S C & Schultz S, *Phys Rev Lett*, 84 (2000) 4184.
3 Smith D R, Pendry J B & Wiltshire M C, *Science*, 305 (2004) 788.
4 Padilla W J, Basov D N & Smith D, *Mater Today*, 9 (2006) 28.
5 Shelby R A, Smith D R & Schultz S, *Science*, 292 (2000) 77.
6 Pendry J B, *Phys Rev Lett*, 85 (2000) 3966.
7 Pendry J B, Schurig D & Smith D R, *Science*, 312 (2006) 1780.
8 Schurig D, Mock J J, Justice B J, Cummer S A, Pendry J B, Starr A F & Smith D R, *Science*, 314 (2006) 977.
9 Palandöken M, *Artificial materials based microstrip antenna design, in microstrip antennas*, Edited by Nasimuddin N, (InTech), 2011.
10 Palandöken M, *Microwave Opt Technol Lett*, 58 (2016) 1404.
11 Upadhyaya T K, Kosta, S P, Jyoti R & Palandöken M, *Opt Eng*, 53 (2014) 107104.
12 Upadhyaya T K, Kosta S P, Jyoti R & Palandöken M, *Int J Microwave Wirel Technol*, 8 (2016) 229.
13 Palandöken M & Sondas A, *Microwave J*, 57 (2014).
14 Palandöken M & Ucar M H, *Microwave Opt Technol Lett*, 56 (2014) 2903.
15 Palandöken M, *Metamaterial-based compact filter design in metamaterial*, Edited by Jiang X Y, (InTech), 2012.
16 Caloz C & Itoh T, *Electromagnetic metamaterials: Transmission line theory and microwave applications*, (John Wiley & Sons), 2005.
17 Landy N I, Sajuyigbe S, Mock J J, Smith D R & Padilla W J, *Phys Rev Lett*, 100 (2008) 207402.
18 Sharma S K, Ghosh S, Srivastava K V & Shukla, A, *Microwave Opt Technol Lett*, 59 (2017) 348.
19 Sood D & Tripathi C C, *J Microwaves, Optoelectron Electromagn Appl*, 16 (2017) 514.
20 Ramya S & Srinivasa Rao I, *Microwave Opt Technol Lett*, 59 (2017) 1837.
21 Baskey H B, Akhtar M J, Dixit A K & Shami T C, *J Electromagn Waves Appl*, 29 (2015) 2479.
22 Wang N, Tong J, Zhou W, Jiang W, Li J, Dong X & Hu S, *IEEE Photon J*, 7 (2015) 1.

23 Agarwal M, Behera A K & Meshram M K, *Electron Lett*, 52 (2016) 340.

24 Sood D & Tripathi C C, *J Electromagn Waves Appl*, 31 (2017) 394.

25 Wang B X, Wang L L, Wang G Z, Huang W Q, Li X F & Zhai X, *IEEE Photon Technol Lett*, 26 (2014) 111.

26 Bhattacharyya S, Ghosh S, Chaurasiya D & Srivastava K V, *IET Microwaves, Antennas Propag*, 9 (2015) 1160.

27 Ghosh S, Bhattacharyya S, Kaiprath Y & Vaibhav Srivastava K, *J Appl Phys*, 115 (2014) 104503.

28 Bhattacharyya S, Ghosh S, Chaurasiya D & Srivastava K V, *Appl Phys A*, 118 (2015) 207.

29 Agarwal, M, Behera, A K & Meshram, M K, *Appl Phys A*, 122 (2016) 166.

30 Wang G D, Chen J F, Hu X, Chen Z Q & Liu M, *Progress Electromagn Res*, 145 (2014) 175.

31 Dincer F, Karaaslan M, Unal E, Akgol O, Demirel E & Sabah C, *J Electromagn Waves Appl*, 28 (2014) 741.

32 Kaur K P, Upadhyay T K & Palandoken M, *Progress Electromagn Res C*, 77 (2017).

33 Liu R, Cui T J, Huang D, Zhao B & Smith D R, *Phys Rev E*, 76 (2007) 026606.

34 Ostaffe H, 'RF-based wireless charging and energy harvesting enables new applications and improves product design', 2012, Available at: http://www.mouser.in/applications/rf_energy_harvesting/

35 Smith D R, Vier, D C, Koschny T & Soukoulis C M, *Phys Review E*, 71 (2005) 036617.

36 Chang K, Martin S, Wang F & Klein J L, *IEEE Trans Microwave Theory Tech*, 35 (1987) 1288.

37 Tao H, Landy N I, Bingham C M, Zhang X, Averitt R D & Padilla W J, *Opt Exp*, 16 (2008) 7181.

38 Huang L & Chen H, *Progress Electromagn Res*, 113 (2011) 103.

39 Kaur K P & Upadhyaya T, *IET Microwaves, Antennas Propag*, 12 (2018) 1428.

40 Li L, Yang Y & Liang C, *J Appl Phys*, 110 (2011) 063702.

41 Zhai H, Zhan C, Liu L & Zang Y, *Electron Lett*, 51 (2015) 1624.